# Application of an improved vegetation index from the visible spectrum in the diagnosis of degraded pastures: Implications for development

Thiago Luiz da Silva Quinaia[a], Renato Farias do Valle Junior[a], Victor Peçanha de Miranda Coelho[a], Rafael Carvalho da Cunha[a], Carlos Alberto Valera[b], Luís Filipe Sanches Fernandes[c], Fernando António Leal Pacheco[d,*]

[a]Federal Institute of Triângulo Mineiro, Uberaba Campus, Geoprocessing Laboratory, Uberaba, MG 38064-790, Brazil. thiagoquinaia@hotmail.com, renato@iftm.edu.br, victorcoelho@iftm.edu.br, rccunha@gmail.com

[b]Regional Coordination of the Environmental Justice Prosecutor's Office of the Paranaíba and Lower Rio Grande River Basins, Coronel Antônio Rios Street, 951, Uberaba, MG 38061-150, Brazil. carlosvalera@mpmg.mp.br

[c]Center for Research and Agro-environmental and Biological Technologies, University of Trás-os-Montes e Alto Douro, Ap. 1013, 5001-801 Vila Real, Portugal. lfilipe@utad.pt

[d]Center of Chemistry of Vila Real, University of Trás-os-Montes e Alto Douro, Ap. 1013, 5001-801 Vila Real, Portugal. fpacheco@utad.pt

(*) corresponding author

## ABSTRACT

Inadequate pasture management causes land degradation and negative impacts on the socio-economic development of agricultural regions. Given the importance for Brazil and the World of pasture-based livestock production, the recognition of pasture degradation is essential. The use of remote sensing satellite systems to detect degraded pastures increased in the recent past, because of their capability to survey large portions of Earth's surface. A struggle nowadays is to improve detection accuracy and to implement high-resolution surveys at farmland scale using unmanned aerial vehicles (UAVs). The satellite sensors capture reflectance from the visible spectrum and near infrared bands, which allows estimating plant's vigor vegetation indices. The NDVI is a widely accepted index, but to generate an NDVI map using a UAV a relatively high-cost multispectral sensor is required, while most UAVs are equipped with low-cost RGB cameras. In the present study, a script developed on the Google Earth Engine image-processing platform manipulated images from the Landsat 8 satellite, and compared the performances of NDVI and an improved color index that we coined "Total Brightness Quotient" of red (TBQR), green (TBQG) and blue (TBQB) bands. An efficient detection of pasture degradation using the TBQs would be a good prognosis for the surveys at farm scale where environmental authorities are progressively using UAVs and forcing landowners towards pasture restoration. When compared to NDVI, the TBQG showed a correlation of 0.965 and an accuracy of 88.63%. Thus, the TBQG proved as efficient as the NDVI in the diagnosis of degraded pastures.

*Keywords:* Remote sensing; Unmanned aerial vehicles; Google Earth Engine; Total Brightness Quotient; NDVI; Pasture degradation

## 1. INTRODUCTION

The nutrients required by animals are 90% obtained from pastures (Euclides et al., 2010). Notwithstanding the importance of pastures for feeding, around 108 million hectares of existing fenced pastures in Brazil are degraded or in degradation (Embrapa, 2014; Embrapa Territorial, 2018), which means 60% of pastureland in this country.

Pasture degradation is a slow gradual process. It reduces plant vigor and hence the capacity of forage plants to sustain the production and quality demanded by the animals. It also weakens the resilience to pests, diseases and the invasion by non-palatable species (Zhumanova et al., 2018), which increases the chances of advanced degradation (Zimmer et al., 2012). A possible cause of pasture degradation is the lack of conservation practices (Rocha Junior et al., 2016), namely adjustment of grazing rates (Dias, 2014; Fernandes et al., 2018; Postel, 1998), and the grazing on slopes > 20º, which can negatively affect soil stability and increase erosion (Torres et al., 2019).

The causes of pasture degradation are well known, but their spatial and temporal dynamics remain poorly understood (Neves, 2017). An approach used to shed light over this issue relies on the coupling of remote sensing and geographic information systems, whereby the reflectance of pastures captured by sensors in cameras are used to estimate vegetation indices that correlate with the vigor of plants (Lu and Weng, 2007; Novo and Ponzoni, 2001; Torres et al., 2019). The spectral response of pastures is difficult to grasp because it depends on many factors, such as species assemblage, soil type or precipitation, which makes it extremely complex to classify pasture degradation using vegetation indices (Davidson et al., 2008). Nevertheless, several authors have used orbital sensors to analyze and map spatial and temporal variations in pasture fields using these proxies. The Normalized Difference Vegetation Index (NDVI) was the most widely used indicator (Imukova et al., 2015; Li S. et al., 2012; Li X. et al., 2012; Torres et al., 2019; Valle Júnior et al., 2019; Wiesmair et al., 2016). Other frequently used indexes include the Enhanced Vegetation Index, EVI (Junges et al., 2016; Karnieli et al., 2013); the Soil-Adjusted Vegetation Index, SAVI (Batista et al., 2020); the Leaf Area Index, LAI (Batista et al., 2020; Chen et al., 2019; Wang et al., 2019); the Water Use Efficiency, WUE (Fernandes et al., 2018); the Net Primary Productivity, NPP (Fernandes et al., 2018; Jiang et al., 2019; Sun et al., 2019); among others.

Many authors have also applied visible spectrum sensors (RGB) to quantify and map indicators of plant's biophysical state, such as above ground biomass, plant vigor, productivity and the Leaf Area Index (Córcoles et al., 2013; Jang et al., 2020; Kim et al., 2019; Liu and Pattey, 2010). Other studies indicated the RGB-based color vegetation index and the excess of green index, to diagnose vegetation cover (Arroyo et al., 2016; Beniaich et al., 2019). The green leaf index, on the other hand, proved efficient to count plants (Louhaichi et al., 2001; Silva, 2017), distinguish plant biomass from soil and residue (Meyer and Neto, 2008), monitor vegetation fraction (Marcial-Pablo et al., 2019), and estimate the Leaf Area Index as well as key growth indicators of rice (Li et al., 2019; Qiu et al., 2020). However, to our best knowledge no study attempted to diagnose pasture degradation using a RGB index. Eventually, the ease of obtaining reflectance data from the near infrared band using orbital satellites such as Sentinel 2, Landsat 8 or MODIS, hampered the development of such studies. However, comparing the detection efficiency among the visible (RGB) and near infrared (NIR) ranges would help to shed light on the potential of each range. Besides, the use of visible range vegetation indexes could boost the use of low-cost monitoring equipment, such as unmanned aerial vehicles (UAV) at the canopy level and even smart phones at the leaf level, which comprise RGB but rarely NIR cameras (Costa et. al., 2020).

The general purpose of this study was therefore to detect degraded pastures using the NDVI and the RGB-based Color Index (CI) of Woebbecke et al. (1995), comparing the performances in the sequel. As corollary, we aimed to improve the CI index for detection efficiency. The normalization through simple ratio processes applied to most vegetation indexes (Katsoulas et al., 2016) inherently generates asymptotic approaches to saturation shrinking the range of linear relation between the index and biophysical characteristics and hence the index's detection capacity (Gitelson, 2004). For example, the ratio between the difference and the sum used in the NDVI equation [(ρNIR – ρred) / (ρNIR + ρred)] is barely capable to describe the plant vigor when the target areas present high biomass (e.g., vegetation fraction > 60%). In these cases, the ρNIR / ρred ratio > 1, both the numerator and denominator get close to equivalence and the sensitivity of NDVI to ρNIR becomes insignificant. The generalization caused by difference over sum normalization also affects the CI.

Thus, by applying changes in the denominator of the vegetation index called the Color Index - CI (Woebbecke et al., 1995), the influence of the normalization process can be eliminated. For the CI, the normalization process happens with the ratio between the target band and the sum of all (BGR) (B = ρblue / (ρred + ρgreen + ρblue); G = ρgreen / (ρred + ρgreen + ρblue); R = ρred / (ρred + ρgreen + ρblue)). This causes a drop in sensitivity when the ρnumerator / sum of all (BGR) ratio denominator > 1, as noted in Gitelson (2004). Therefore, the only way to increase the sensitivity of the CI is to change the denominator of the original equation. For this reason, we developed the "Total brightness quotients" of Blue (TBQB), Green (TBQG) and Red (TBQR) as part of our goal for this study.

## 2. MATERIAL AND METHODS

### 2.1. Study area

The study was carried out in the Environmental Preservation Area - EPA of the Uberaba River Basin (Fig. 1), which was declared in 1999 (Minas Gerais State Law No. 13,183 / 1999) and later the municipality of Uberaba also edited the Municipal Law 9,892 / 2006, which Creates the Municipal Environmental Protection Area of the Uberaba River – EPA of Uberaba River - and takes other measures because it is fundamental for the protection of water resources, the riverside ecosystem, fauna and remnants of native vegetation (*Savanna* Biome). It occupies an area of approximately 52810.80 hectares and protects the Uberaba River located between the geographical coordinates 19.51 - 19.74° south and 47.64 - 47.98° west of Greenwich, which in turn provides 95% of the drinking water demanded by the municipality, which has about 295,988 inhabitants (IBGE, 2020; PMU and CODAU, 2006).

The climate in the EPA is Aw, described as tropical hot and humid with a cold, dry winter (Beck et. al., 2018). The climatic domain is said to be semi-humid with low precipitation for 4-5 months of the year, with the annual precipitation varying between 1300 and 1700mm. The rainy period corresponds to the hottest season of the year from October to March, with the dry season from April to September. Precipitation is more intense in December and January (Abdala, 2012).

The EPA's lithostratigraphic sequence is comprised of the Serra Geral (volcanic), Uberaba and Marília (sedimentary) formations (Fig. 2), which form the Bauru Group of the Cretaceous (Cruz, 2003). Most types of soil in this plateau are characterized by medium texture that varies from sandy to clayey and has different levels of fertility (Nishiyama, 1998). According to the FAO classification, these types of soil are called Latosols, Argisols and Gleisols (Siqueira et al., 2017).

55.45% of the EPA area is occupied by natural and planted pastures, predominated by the species Brachiaria Brizantha cv. Marandú. In the Serra Geral, Marília and Uberaba geological formation we find 8183.43; 4882.53; 16219.72 ha, respectively (Table 1).

**Place Figure 1 here**

**Place Figure 2 here**

**Place Table 1 here**

### 2.2. Data acquisition and preparationn

The sources of data used to perform the pasture degradation modeling are listed in Table 2. The soil fertility and resistance to penetration analyses were based on field data, obtained as described below (item 2.3). To delimit the pasture areas within the EPA, the land use and occupation map provided by Mapbiomas referring to collection 5 of the year 2019 was used. Following that, the delimitation of the geological formations was obtained through the map provided by the State System of Environment and Water Resources. In order to compare the detection efficiency (item 2.6) between the vegetation indices of the visible TBQB, TBQG, TBQR and NDVI, 32 images from the Landsat 8 OLI / T1_SR Satellite with a 15-day temporal and 30-meter spatial resolution were used through the years 2017–2019. The 32 images were processed in the cloud and used to extract the zonal statistics (mean, minimum, maximum and standard deviation) of each of the 6 ground truth locations in spreadsheet format, separated by geology and vegetation indexes (item 2.6). Afterwards, regression, correlation (Minitab® 19) and sensitivity analysis (Excel®) were carried out in order to compare the efficiency of vegetation indices in detecting degraded pasture (item 2.5). With the images collected, a total of 12 degraded pasture maps were made using the programming presented in item 2.4, one map for each vegetation index (TBQB, TBQG, TBQR and NDVI) in each geology (Serra Geral, Uberaba and Marília).

**Place Table 2 here**

### 2.3. Identification of phytophysiognomies in the pastures

The signs of pasture degradation are not always visible, making it difficult to detect the primary cause of degradation, as it causes a chain reaction. The frequency of invasive plants, the density of forage plants and the percentage of soil cover by desirable plants are parameters that can be used for evaluation. The degradation of pastures in their most advanced stages is characterized by changes in the dynamics of the plant community, where desirable species (forage plants) give way to others, of lesser or almost no forage value, and by the decline in forage productivity, with reflects in animal production (Townsend et al., 2012).

According to Macedo et al. (2014) the state of degradation of the pasture can be identified by physiological factors of the plant and, also, of the soil. In the plant, the regrowth capacity, height of the pasture, presence of areas without vegetation and inhomogeneous coverage, infestation of invasive plants and pests are observed. While in the soil, the effect of compaction, erosion, and mineral deficiencies, mainly of Nitrogen and Phosphorus, are verified (FAO, 2009).

In this sense, diligence was taken in the field of the study area to identify the pasture phytophysiognomies, in order to characterize and georeference two training points in terms of geological formation, called: healthy pasture and degraded pasture. As a visual basis the characteristics of Fig. 3 show the healthy pasture has green and tall grass with homogeneous coverage and the degraded pasture with areas of exposed soil and the presence of invading species and termite mounds.

**Place Figure 3 here**

These two phytophysiognomies were characterized at a field level in terms of soil fertility and physical parameters, at 6 ground truth locations, distributed in the three geological formations Serra Geral, Uberaba and Marília.

Each of these ground truth sites is represented by a 50-meter buffer (0.7853 ha) centered on the point where phytophysiognomy is most representative. The 6 selected ground truth sites are represented in Fig. 2 as *characterization ground truth sites*. They were georeferenced with a Garmim GPSMAP® 78 receiver. In each of these locations, 4 soil samples were collected at random at a depth of 0-0.2m and used to perform chemical and physical analyzes in a specialized laboratory. Also, at these locations, 7 random resistance to penetration samples were made with the digital penetrometer PLG 1020 penetroLOG® (Falker Automação, Porto Alegre, RS) at a depth of 0-0.6m. The soils of the geological formations were characterized chemically and physically and presented by Valle Junior et al. (2019).

## 2.4. Programming in Google Earth Engine (GEE)

The zonal statistics and coincidence maps were generated in each geological formation, from 32 images from the Landsat 8 OLI / T1_SR from the years 2017, 2018 and 2019. The processing was performed in a routine prepared in Javascript in the GEE code editor menu, which has a public catalog with millions of images on a planetary scale (GEE, 2020; Gorelick et al., 2017).

The first script called "Zonal Statistics" is available at:

https://code.earthengine.google.com/85c7e8d6904f747ad848d11504bae53f

and the second "Map of Coincidence" is available at:

https://code.earthengine.google.com/e4a6f8aafd4216631d950a538fac3020.

Therefore, GEE emerges as a facilitator in the search for images, enabling the automatic cropping of images based on the area of interest, filter by analysis period, calculation of NDVI, TBQB, TBQG and TBQR, extraction of zonal statistics, export of data in raster format and spreadsheet. The operational details relative to the GEE scripts are illustrated in Fig. 4 and described in the Supplementary Material.

**Place Figure 4 here**

## 2.5. Map of degraded pasture using the vegetation indexes TBQB, TBQR, TBQG and NDVI

Based on the methodology proposed by Valle Junior et al. (2019), we used pre-established training samples in the field (ground truth locations) for supervised classification of orbital images. After determining the interval between the minimum and maximum reflectance values of the NDVI vegetation index for each buffer, the image was binarized (item 2.4) and the sum of the image collection, generating the number of pixel matches by similarity with the training sample intervals. Thus, values above 4 coincidences were considered similar, with an accuracy level of 84.1%.

In this work, we used images from the Landsat 8 OLI / T1_SR orbital satellite processed in the cloud on the GEE platform, from the development of two scripts (item 2.4). The first script was designed to filter images with < 30% clouds from the years 2017, 2018 and 2019, apply the vegetation index to the series of images, calculate zonal statistics and export information for statistical modeling in MINITAB 19®. The second generated script, automates the method proposed by Valle Junior et al. (2019), generating a pixel coincidence map for each NDVI, TBQB, TBQG and TBQR vegetation index (equations 3, 4, 5 and 6) and geological formation (Serra Geral, Uberaba and Marília).

The visible vegetation indexes (TBQB, TBQG and TBQR) come from a change in the denominator of the Color Index (CI) (Woebbecke et al., 1995) according to equations 7, 8 and 9. Therefore, they present the amount of reflectance that was reflected from Blue (TBQB), Green (TBQG) and Red (TBQR) taking into account the portion that was reflected by the other bands.

$$NDVI=\frac{NIR-¿}{NIR+¿}(3)$$

$$TBQB=\frac{¿}{(¿+¿)}(4)$$

$$TBQG=\frac{¿}{(¿+¿)}(5)$$

$$TBQR=\frac{¿}{(¿+¿)}(6)$$

$$B=\frac{¿}{(¿+¿+¿)}(7)$$

$$G=\frac{¿}{(¿+¿+¿)}(8)$$

$$R=\frac{¿}{(¿+¿+¿)}(9)$$

## 2.6. Seasonality of vegetation indices

Equations were drawn up that represent the seasonal variation of the vegetation indices throughout the year, enabling the comparison of pasture phytophysiognomies in the geological formations. For that, we used the vegetation indices as a dependent variable in the model and the days of the year (DOY) as an independent variable to estimate the seasonality of the vegetation indices in the dry and rainy period to diagnose the phytophysiognomies of healthy and degraded pastures. Thus, equations were modeled in the MINITAB 19 software, using the General Linear Model - GLM method, to determine the adjusted determination coefficient (adjusted R2) and standard deviation of the distance between the real and adjusted values (S).

From the average values of the vegetation indices, the Spearman correlation coefficient was calculated, which measures the intensity of the relationship between two variables. In addition, time series graphs were drawn up to show dispersion of the average values of each vegetation index and its seasonality over the years.

*2.6.1. Sensitivity of equations*

In the analysis of the reflectance of the vegetation indices in the phytophysiognomies from the regression equations generated in item 2.6, the sensitivity analysis of the equations was carried out as a comparison between the indices. Following the methodology proposed by Gitelson (2004) that measures the possible sensitivity between vegetation indices in identifying biophysical changes in plant targets, the following expressions were used:

$$Sb=\frac{d(TBQB)}{d(NDVI)}\times\left(\frac{1}{\frac{\Delta TBQB}{\Delta NDVI}}\right)(10)$$

$$Sg=\frac{d(TBQG)}{d(NDVI)}\times\left(\frac{1}{\frac{\Delta TBQG}{\Delta NDVI}}\right)(11)$$

$$Sr=\frac{d(TBQR)}{d(NDVI)}\times\left(\frac{1}{\frac{\Delta TBQR}{\Delta NDVI}}\right)(12)$$

Where, Sb (TBQB Sensitivity), Sg (TBQG Sensitivity), Sr (TBQR Sensitivity), d (TBQB), d (TBQG), d (TBQR) and d (NDVI) are the first derivatives of each of the equations (item 2.6) and ΔTBQB = TBQBmax - TBQBmin; ΔTBQG = TBQGmax - TBQGmin; ΔTBQR = TBQRmax - TBQRmin and ΔNDVI = NDVImax - NDVImin, are the intervals of the observed values of each vegetation index, that is, the difference between the maximum and minimum values of each index. Therefore, Sensitivity (S) values < 1 indicate that NDVI is more sensitive than the visible index. When S = 1, the sensitivities between the indices are the same. Values of S > 1 indicate that the visible index is more sensitive than the NDVI.

## 2.7. Detection efficiency of degraded pastures

To measure the detection efficiency of the visible with the NDVI in the detection of degraded pasture, we evaluated the variable responses of the tests using: a) Cross analysis (item 2.7.1); b) Ground truth validation (item 2.7.2).

*2.7.1. Cross analysis (Crosstab)*

From the degraded pasture maps (item 2.4), a cross analysis was performed between the maps generated with the visible indices and the NDVI, in order to quantify similar and surplus areas. In this sense, the greater the intersection and the lesser the exception between the maps, the better its efficiency. We use the CROSSTAB tool from QGIS 3.10.5.

*2.7.2. Validation of degraded pasture maps*

In the validation of the degraded pasture maps generated from the vegetation indices, the limits of resistance classes were used as a reference in the diagnosis of degradation (Valle Junior et al., 2019) in each of the geological formations, 4428.5 ± 1271.2 kPa, 5418.3 ± 700.5kPa and 5464.9 ± 1037.3 kPa referring to Serra Geral, Marília and Uberaba, respectively. Thus, in field collections, resistance to penetration was measured at random in the study area. In total, 38 checkpoints were collected (Fig. 1). The measurements were performed at a depth of 0 to 0.6 m, using a penetrometer model PLG 1020 penetroLOG manufactured by the company Falker Automação. With the resistance values, the degradation classification was generated, calculating the percentage of correctness in each geology.

## 3. RESULTS

### 3.1. Equations for time series of vegetation indices and detection sensitivity

The best adjustment for the regression that models the spectral variations of the vegetation indices throughout the year was the cubic with a significance of $p < 0.05$ in all geological formations. For degraded pasture, the adjusted determination coefficient ($R^2$aj.) for the Serra Geral, Marília and Uberaba geological formations of the indices were: NDVI 72.78%, 84.27%, 82.22%; TBQB 65.01%, 41.26%, 48.01%; TBQG 77.85%, 80.80%, 81.25% and TBQR 72.82%, 77.81%, 83.92%, respectively. While in the healthy pastures the indices were: NDVI 65.22%, 86.42%, 78.52%; TBQB 64.07%, 49.12%, 53.13%; TBQG 73.93%, 83.15%, 85.17% and TBQR 67.63%, 81.63%, 79.87%, respectively, (Figs. 5a, 5b, 5c and 5d). The classification of $R^2$aj. for the $R^2$aj. range was from 0 - 0.09 (weak determination), 0.09 - 0.49 (average), 0.49 - 0.81 (strong), 0.81 - 0.9801 (very strong) and 0.9801 - 1 (perfect) (Sanchez, 2013). To assess the acceptance of the adjustments, the adjusted determination coefficient ($R^2$aj.) was used as criteria, as well as the standard deviation of the distance between the real and adjusted values (S) (Araujo, 2019; Quinino et al., 1991). In this way, the $R^2$aj. for the models applied to degraded and healthy pasture, in the Serra Geral, Marília and Uberaba formations using NDVI presented classification varying from strong to very strong, TBQB medium-strong, TBQG and TBQR from strong to very strong. In the regression there was a high $R^2aj$ value with a low S value indicating that the day of the year (DOY) predictor is related to the changes in the vegetation indices (IV) response variable available (Figs. 5a, 5b, 5c and 5d). The spectral behavior over the years does not have a normal distribution, and therefore was evaluated for similarity between the indices using the Spearman test ($p < 0.05$). The coefficient classification (rs) was classified for the rs range from 0 - 0.40 (bad correlation), 0.40 - 0.60 (low correlation), 0.60 - 0.80 (average correlation), 0.80 - 0.90 (good correlation) and 0.90 - 1.0 (high or excellent correlation) (Martins and Domingues, 2014). Thus, the correlations in the geological formations Marília, Serra Geral and Uberaba between the TBQB, TBQG and TBQR indices with the NDVI were -0.524, 0.966, -0.966; -0.794, 0.965, -0.956; -0.723, 0.989, -0.984. Thus, in all the geological formations analyzed, the best fit was found for the TBQG (direct correlation), followed by the TBQR (indirect correlation), both presenting high or excellent classification, while the TBQB (indirect correlation) varied from low to medium.

**Place Figures 5 here**

*3.1.1 Comparison between amplitude and deviation of time series of vegetation indices*

When assessing the seasonal variation between the years 2017 to 2019, the trend of similar behavior of the NDVI and TBQG indices was observed, differing from the G (see Supplementary Material Figs. S1a, S1b, S1c, S1d, S1e, and S1f). Therefore, the amplitude and deviations of the values corresponding to the NDVI and TBQG indices were close, which suggests that there is less sensitivity of equation G in capturing the biophysical changes of pasture in the period (see Supplementary Material Tables S1a, S1b and S1c).

**3.2. Maps of degraded pastures**

The raster files in TIFF format extracted from GEE and finished in the GIS (Figs. 6a, 6a1, 6b, 6b1, 6c and 6c1), refer to the degraded pasture maps generated through each vegetation index NDVI, TBQ, TBQG and TBQR in the different geologies. The degraded pasture areas mapped using each index follow as shown in Table 3. We can see that in the EPA degraded pasture occupies an area of 12,066.93, 25,180.11, 18,985.32 and 17,486.28 hectares diagnosed by the indices NDVI, TBQB, TBQG and TBQR, respectively. Representing a percentage of 41.20%, 85.98%, 64.83%, 59.71%, respectively, in relation to the total pasture area according to land use and occupation.

**Place Figures 6 here**

**Place Table 3 here**

The sensitivity of the models (Sb, Sg, Sr) was calculated on the targets in the degraded pasture in the Serra Geral, Marília and Uberaba geological formations to compare the indices. TBQB (-0.67, 0.77 and -0.75); TBQG (-0.51, 0.65 and -0.68) and TBQR (-0.08, 0.29 and -0.46) were compared to the NDVI model and resulted in an S <1. Therefore, by this method the NDVI was classified as the most sensitive index. In addition, as an innovation in this study, we quantify the difference in sensitivity between the modified indices developed using RGB compared to NDVI in relation to the diagnosis of degraded pasture.

The time series of vegetation indices over the three years (see Supplementary Material Figs S2a, S2b, S3a, S3b, S4a and S4b) shows that TBQG generates higher values than NDVI with a smaller amplitude, but higher than TBQR and TBQB. In the sequence, the TBQR inversely follows the NDVI with equivalent values and less amplitude than the NDVI and TBQG. Finally, TBQB inversely follows NDVI with lower values and an amplitude smaller than all evaluated.

In addition, the average values of S and R2(aj) of the general regression models of degraded pasture for each vegetation index were NDVI (0.066 - 79.76%), TBQB (0.014 - 51.43%), TBQG (0.055 - 79.97%), TBQR (0.023 - 78.18%), respectively. Thus, it was possible to associate the predicted values of biophysical state of the pasture with observed values in the time series.

The areas obtained by the modified vegetation indices (RGB) were greater, as seen in the Supplementary Material (Table S2). In the identification of the degraded pasture, a pixel coincidence greater than 4 (four) or more was observed in the band of the visible spectrum in the interval between the values (Min and Max) of the sample polygons.

The increase in the number of coincidences refers to the number of times in which another pixel, outside the sample polygon, was within the minimum and maximum observed range of each collected image. Therefore, we observed that the lower sensitivity of the RGB indices favored the increase in pixel coincidences and the consequent increase in the area of mapped degraded pasture.

As a verification of the actual state of the field (ground truth) according to Valle Júnior et al. (2019), degraded pasture can be diagnosed from the resistance to penetration in the geological formations – Serra Geral 4428.5 ± 1271.2 kPa, Marília 5418.3 ± 700.5kPa and Uberaba 5464.9 ± 1037.3 kPa. Therefore, in the validation of the degraded pasture maps in the field, by means of the percentage of correctness between the ground truth points and the degraded pasture maps there was agreement of 65.79% with NDVI, 60.53% with TBQB, 65.79% with TBQG and 65.79% with TBQR, which according to Landis; Koch (1977) can be classified as substantial agreement, which is very good.

### 3.3. Cross tabulation results

In the cross analysis between the maps of degraded pasture established by the vegetation indices NDVI, and RGB (TBQB, TBQG, TBQR) it was possible to verify the percentage of common areas of pasture degradation to assist in map validation. The pixel coincidence between the NDVI and the modified RGB indices tested, demonstrated different behavior in the geological formations. In the Marília, Serra Geral and Uberaba formation there was a minimum pixel match of 90.44; 87.05; 89.43%, respectively, which is excellent. This is presented in the Supplementary Material (Table S3). However, the visible spectrum indices overestimated, on average, the degraded pasture area in all formations – 13.46% for TBQB, 6.40% for TBQG and 4.97% for TBQR. However, for the TBQG and TBQR indices, in the field they were as accurate as NDVI, suggesting that the mapped areas can be accepted.

## 4. DISCUSSION

The modified RGB indices, named as the total brightness quotient, of the blue, green and red spectral bands, captured different characteristics for each geological formation and phytophysiognomy of the pasture. Thus, the targeted plants absorbed the light differently for each band of the visible spectrum, according to its edaphoclimatic status and geology.

The relationship between the areas of geomorphology and pedology are closely interdependent (Rubira et al., 2019). This mutual dependence does not allow us to judge that the geology of a region fully explains its pedogenesis, or the other way around. According to Nakashima et al., 2017, even if there is a baseline difference between geological formations, pedogenetic processes are responsible for altering the marks of older and more extensive events, causing a new physiognomy to the landscape. In the study area we have the Serra Geral formation represented by basalt with intercalations of sandstone and diabase dikes (CPRM, 2014). The Marília formation represented by sandstone, conglomerate and paleosol strongly cemented by $CaCo_3$ and $SiO_2$, while the Uberaba formation consists of sandstone, mudstone, siltstone and conglomerate rock (Batezelli, 2015). Therefore, there are several types of soil within each geology, such as dystrophic and dystrophic red latosols, dystrophic red-yellow latosols, eutrophic red argisol and dystrophic melanic gleysol (UFV, 2010). The differences in sensitivity between the vegetation indices of the mapped areas of degraded pasture occur due to the influence of different geologies with different levels of iron oxides present in the clay fraction, as well as the various types of soil and plant physiology. The reflection of light by the soil is a property widely used in pedology and is based on color (Netto and Baptista, 2000), which helps soil classification (Santos et al., 2018), differentiates erodibility (Dantas et al., 2014), evaluates the productive potential (Carmo et al., 2016) and even estimates chemical parameters (Cruz et al., 2018). Therefore, each geology with its own characteristics contributes and changes the perception of each vegetation index used. According to Meneses et al. (2019) the minimal variations in composition or percentage variation of minerals is enough to cause different spectral responses. The concentrations of iron oxides in the Serra Geral formation (Silva et al., 2020), due to the hematite content in the clay fraction (Mello et al., 2003), promote better soil aggregation and water use (Correa et al ., 2008) and promote less resistance to soil penetration (Valle Junior et al., 2019). In addition, they alter the visible spectral response of the soil (Canti and Linford, 2020).

The energy source for photosynthesis and plant growth is light (Bayat et al., 2018). And through several photoreceptor pigments in the plant regulates its growth and development. Light promotes and triggers various morphogenic and physiological processes (Chen et al., 2004). The visible colors are the result of the interaction of light with the retina, where absorption and selective reflection are the reason that most objects are colored (Netto and Baptista, 2000). However, the chlorophyll molecules present in plant cells are more efficient at absorbing the red and blue bands of the spectrum compared to green (Taiz and Zeiger, 2017).

The time series of the vegetation indices show that pasture in the dry period has a general tendency to decrease reflectance in TBQG and NDVI and increased reflectance in TBQR, regardless of the geological formation and the condition of the pasture (healthy or degraded). The reflectance of the TBQB followed the pattern of the TBQR, but with lower peaks. In the rainy season, the reflectance pattern of the pasture was the opposite, with an increase in reflectance in TBQG and NDVI and a decrease in reflectance in TBQR and TBQB. Thus, green (TBQG) achieved a better correlation with NDVI, presenting similar amplitude and deviation.

The strong absorption of light by photosynthetic pigments dominates the optical properties of green leaves in the visible spectrum (400-700 nm). Thus, the decrease in the photosynthetic pigment content of the leaf causes an increase in reflectance and transmittance in the visible spectrum (Jacquemoud and Ustin, 2008).

Water stress and nutrient deficiency (e.g. nitrogen) are highly related to the decrease in chlorophyll content, and consequently less radiation is used by the plant. These stresses are common in dry periods in tropical environments, especially in degraded pastures. In addition to physiological disturbances as a consequence of stress, less biomass and changes in the architecture of the plants in the pasture during the dry season are also expected. Several authors (Merzlyak et al., 2003; Jain et al., 2007; Sclemmer et al., 2005; Vigneau et al., 2011) observed a strong correlation between chlorophyll content and reflectance of crops in the 640-660 ranges nm or Red-Edge (both in red), so that the decrease in chlorophyll content results in an increase in the reflectance of red (Katsoulas et al., 2016). The data found in the literature corroborate the results of pasture reflectance in the dry period of the present study (decrease in TBQG and NDVI and increase in TBQR); which is probably related to the decrease in chlorophyll content. Additionally, the decrease in TBQG and NDVI of the pasture in the dry season may also have been influenced by other factors, such as leaf thickness, age and leaf angle, leaf area index and biomass (Peñuelas and Filella, 1998; Katsoulas et al., 2016).

The use of vegetation indices from the visible spectrum, TBQR and TBQG, are efficient in monitoring pasture development. In addition, the utilization of each pigment (photosynthesizer, photoreceptor and photoprotector), is correlated with several physiological factors, inherent to each plant species, and edaphoclimatic factors (Ren et al., 2020). That generate several relations between absorbance and reflectance to change its visible color (Sipos et al., 2020). The TBQG and TBQR indices proposed in this work, were able to reach R2ajus and S close to NDVI for the monitoring and diagnosis of degraded and healthy pastures in the study area (see Supplementary Material, Tables S4a, S4b, S4c, and S4d), and with field validation with a similar level of accuracy (Figs. 6a, 6b and 6c), which is good. Other studies have already realized that visible vegetation indices - VIS have sensitivity to monitor the biophysical parameters of targeted plants (Jang et al., 2020; Liu and Pattey, 2010; Córcoles et al., 2013; Kim et al., 2019; Beniaich et al., 2019; Arroyo et al., 2016; Silva, 2017; Louhaichi et al., 2001). However, none of these were used in the monitoring and diagnosis of degraded pasture. In general, understanding pasture seasonality can contribute to its classification regarding phytophysiognomies. According to Muller et al., 2015, the spectral-temporal classification provides a reliable separation between agricultural land, pastures and natural savanna vegetation. We realized that the TBQR index was able to identify phytophysiognomies (healthy and degraded) efficiently in all geological formations as seen in the Supplementary Material (Figs. S5a, S5b and S5c).

The use of vegetation indices of the visible spectrum proposed in this work, combined with the use of Remote Sensing, are efficient in detecting degraded pasture. In this way, the proposed methodology simplifies the mapping of degraded pasture without using the near infrared band. Therefore, based on this innovation, it will be possible to implement pasture mapping using low-cost cameras embedded or present in UAVs and smartphones. However, in the case of detecting leaf water stress, when the water volume in the soil is low, the plant goes into protection mode and this prevents the diagnosis through visible vegetation indices (Katsoulas et al., 2016).

Therefore, pasture diagnostics is a planning tool that helps in environmental compliance. Thus, so that we do not suffer attacks linked to the issue of agribusiness in Brazil, regarding land occupation, regularly by the European Union and developed countries such as the United States, we need to adapt the policies for the use and occupation of land and water.

The importance of identifying areas of degraded pasture, which under Brazilian law are treated as environmental damage, enables the development of public policies to bring these areas back into the productive system. Usually, they are open areas and have undergone anthropic action (Federal Law 12.651 / 2012 - Brazilian Forest Code).

## 5. CONCLUSION

The use of visible vegetation indices TBQG and TBQR, proved to be efficient when compared to NDVI in the diagnosis of degraded pasture from orbital satellite images, showing that the degraded pasture area in the EPA ranged between 41.20% and 64.83% of the total pasture area. In this way, we can see the great potential that exists in the use of the visible range to reveal the temporal dynamics of the biophysical characteristics of the degraded pasture. With this, the use of visible indexes favors the simplification of the mapping of degradation, favoring the use of low-cost cameras, embedded or present in UAV, orbital satellites and smartphones.

## ACKNOWLEDGMENTS

The present study was carried out within the framework of Conselho Nacional de Desenvolvimento Científico e Tecnológico (CNPq), and of two CNPq active research groups, namely the “Política de Uso do Solo (POLUS) and “Manejo Sustentável de Bacias Hidrográficas” (affiliated to the IFTM). The author affiliated to IFTM, Renato Farias do Valle Júnior, wishes to acknowledge the funding through the CNPq research scholarship Proc. 307921/2018-2. For the author integrated in the CITAB Research Centre, the research was further financed by the National Funds of FCT— Portuguese Foundation for Science and Technology, under the project UIDB/04033/2020. For the author integrated in the CQVR, the research was further financed by National Funds of FCT— Portuguese Foundation for Science and Technology, under the project UIDB/00616/2020.

The authors declare no conflicts of interest. The funders had no role in the design of the study, in the collection, analyses, or interpretation of data, in the writing of the manuscript, or in the decision to publish the results.

# REFERENCES


Abdala, V., 2012. Diagnóstico hídrico do rio Uberaba-MG como subsídio para a gestão das áreas de conflito ambiental. Tese apresentada à Fac. Ciências Agrárias e Veterinárias – UNESP, Câmpus Jaboticabal, como parte das exigências para a obtenção do título Doutor em Agron. (Ciência do Solo).

Abrahão, S.A., Pinto, F. de A. de C., de Queiroz, D.M., Santos, N.T., Gleriani, J.M., Alves, E.A., 2009. Índices De Vegetação De Base Espectral Para Discriminar Doses De Nitrogênio Em Capim-Tanzânia. Rev. Bras. Zootec. 38, 1637–1644. https://doi.org/10.1590/S1516-35982009000900001.

Andrade, T.S., Albertini, T.Z., Barioni, L.G., Medeiros, S.R. de, Millen, D.D., dos Santos, A.C.R., Goulart, R.S., Lanna, D.P.D., 2020. Perception of consultants, feedlot owners, and packers regarding management and marketing decisions on feedlots (Part II): a national survey in Brazil. Can. J. Anim. Sci. 1–36. https://doi.org/10.1139/cjas-2019-0220.

Araujo, I.R.C., 2019. Irrigação com efluente tratado de abatedouro de aves sobre o solo e a produção florestal. Tese apresentada em regime cotutela aos Programa Pós-Graduação em Eng. Agrícola, da Univ. Estadual do Oeste do Paraná, área Conc. em Recursos Hídricos e Saneamento Ambiental e Programa Investig. Agrária y Florestal da Universidade Estadual do Oeste do Paraná.

Arroyo, J., Guijarro, M., Pajares, G., 2016. An instance-based learning approach for thresholding in crop images under different outdoor conditions. Comput. Electron. Agric. 127, 669–679. https://doi.org/10.1016/j.compag.2016.07.018.

Batezelli, A., 2015. Continental systems tracts of the Brazilian Cretaceous Bauru Basin and their relationship with the tectonic and climatic evolution of South America. Basin Res. 29, 1–25. https://doi.org/10.1111/bre.12128.

Batista, P.H.D., Almeida, G.L.P. de, Silva, J.L.B. da, Pandorfi, H., Silva, M.V. Da, Silva, R.A.B. da, Melo, M.V.N. de, Lins, F.A.C., Junior, J.J.F.C., 2020. Short-term grazing and its impacts on soil and pasture degradation. DYNA 87, 123–128. https://doi.org/10.15446/dyna.v87n213.81853.

Bayat, L., Arab, M., Aliniaeifard, S., Seif, M., Lastochkina, O., Li, T., 2018. Effects of growth under different light spectra on the subsequent high light tolerance in rose plants. AoB Plants 10, 1–17. https://doi.org/10.1093/aobpla/ply052.

Beck, H.E., Zimmermann, N.E., McVicar, T.R., Vergopolan, N., Berg, A., Wood, E.F., 2018. Present and future köppen-geiger climate classification maps at 1-km resolution. Sci. Data 5, 1–12. https://doi.org/10.1038/sdata.2018.214.

Beniaich, A., Silva, M.L.N., Avalos, F.A.P., Menezes, M.D. de, Cândido, B.M., 2019. Determination of vegetation cover index under different soil management systems of cover plants by using an unmanned aerial vehicle with an onboard digital photographic camera. Semin. Ciências Agrárias 40, 49. https://doi.org/10.5433/1679-0359.2019v40n1p49.

Canti, M.G., Linford, N., 2000. The Effects of Fire on Archaeological Soils and Sediments: Temperature and Colour Relationships. Proc. Prehist. Soc. 66, 385–395. https://doi.org/10.1017/S0079497X00001869.

Carmo, D.A.B. do, Marques Júnior, J., Siqueira, D.S., Bahia, A.S.R. de S., Santos, H.M., Pollo, G.Z., 2016. Cor do solo na identificação de áreas com diferentes potenciais produtivos e qualidade de café. Pesqui. Agropecuária Bras. 51, 1261–1271. https://doi.org/10.1590/s0100-204x2016000900026.

Chen, M., Chory, J., Fankhauser, C., 2004. Light Signal Transduction in Higher Plants. Annu. Rev. Genet. 38, 87–117. https://doi.org/10.1146/annurev.genet.38.072902.092259.

Chen, Y., Fei, X., Groisman, P., Sun, Z., Zhang, J., Qin, Z., 2019. Contrasting policy shifts influence the pattern of vegetation production and C sequestration over pasture systems: A regional-scale comparison in Temperate Eurasian Steppe. Agric. Syst. 176, 102679. https://doi.org/10.1016/j.agsy.2019.102679.

Coleman, R.W., Stavros, N., Yadav, V., Parazoo, N., 2020. A Simplified Framework for High-Resolution Urban Vegetation Classification with Optical Imagery in the Los Angeles Megacity. Remote Sens. 12, 2399. https://doi.org/10.3390/rs12152399.

Companhia de Pesquisa de Recursos Minerais – CPRM, Serviço Geológico do Brasil, 2014. Mapa Geológico do Estado de Minas Gerais. Ministério de Minas e Energia – Secretaria de Geologia, Mineração e Transformação Mineral. Brasília. Escala 1:1000000.

Córcoles, J.I., Ortega, J.F., Hernández, D., Moreno, M.A., 2013. Estimation of leaf area index in onion (Allium cepa L.) using an unmanned aerial vehicle. Biosyst. Eng. 115, 31–42. https://doi.org/10.1016/j.biosystemseng.2013.02.002.

Correa, M.M., Ker, J.C., Barrón, V., 2008. Caracterização De Óxidos De Ferro De Solos Do. R. Bras. Ci. Solo 1017–1031.

Cruz, L.B.S., 2003. Diagnóstico ambiental da bacia hidrográfica do rio Uberaba-mg. Tese submetida à banca examinadora para obtenção do título Doutora em Eng. Agrícola na área Conc. em Água e Solo.

Cruz, N.N.D.L., Barbosa, R.S., Moura, M.C.S. de, Teixeira, D.D.B., Marques Júnior, J., Silva, J.D.D.F. e, 2018. Color parameters applied to pedotransfer functions in the estimation of soil attributes. Semin. Ciências Agrárias 39, 1479. https://doi.org/10.5433/1679-0359.2018v39n4p1479.

Dantas, J.S., Filho, M.V.M., Marques Júnior, J.M., do Amaral Resende, J.M., de Bortoli Teixeira, D., Barbosa, R.S., Siqueira, D.S., 2014. Coeficiente de erodibilidade em sulcos e entressulcos de Argissolos coesos estimado pela cor do solo. Pesqui. Agropecu. Bras. 49, 700–707. https://doi.org/10.1590/S0100-204X2014000900006.

Davidson, E.A., Asner, G.P., Stone, T.A., Neill, C., Figueiredo, R.O., 2009. Objective indicators of pasture degradation from spectral mixture analysis of landsat imagery. J. Geophys. Res. Biogeosciences 114. https://doi.org/10.1029/2007JG000622.

de Uberlândia - MG. PhD Thesis in Geotechnical. Universidade Federal de São Carlos,

Dias, M.B.F., 2014. Degradação de Pastagens: o que é e como evitar. Brasília, DF.

Dong, Y., Ren, Z., Fu, Y., Miao, Z., Yang, R., Sun, Y., He, X., 2020. Recording Urban Land Dynamic and Its Effects during 2000–2019 at 15-m Resolution by Cloud Computing with Landsat Series. Remote Sens. 12, 2451. https://doi.org/10.3390/rs12152451.

Duarte, E., Barrera, J.A., Dube, F., Casco, F., Hernández, A.J., Zagal, E., 2020. Monitoring Approach for Tropical Coniferous Forest Degradation Using Remote Sensing and Field Data. Remote Sens. 12, 2531. https://doi.org/10.3390/rs12162531.

Empresa Brasileira de Pesquisa Agropecuária – EMBRAPA, 2014. Embrapa Mapeia degradação das pastagens do Cerrado. https://www.embrapa.br/busca-de-noticias/-/noticia/2361250/embrapa-mapeia-degradacao-das-pastagens-do-cerrado. (acesso em 14 de outubro de 2020).

Empresa Brasileira de Pesquisa Agropecuária Territorial - EMBRAPA TERRITORIAL, 2018. Síntese Ocupação e Uso das Terras no Brasil. https://www.embrapa.br/car/sintese. (acesso em 14 de outubro de 2020).

Euclides, V.P.B., do Valle, C.B., Macedo, M.C.M., Almeida, R.G. de, Montagner, D.B., Barbosa, R.A., 2010. Brazilian scientific progress in pasture research during the first decade of XXI century. Rev. Bras. Zootec. 39, 151–168. https://doi.org/10.1590/s1516-35982010001300018.

Fernandes, F.H.S., Sano, E.E., Ferreira, L.G., de Mello Baptista, G.M., Victoria, D. de C., Fassoni-Andrade, A.C., 2018. Degradation trends based on MODIS-derived estimates of productivity and water use efficiency: A case study for the cultivated pastures in the Brazilian Cerrado. Remote Sens. Appl. Soc. Environ. 11, 30–40. https://doi.org/10.1016/j.rsase.2018.04.014.

Flores, J. A., Q. Wu, J., O. Stöckle, C., P. Ewing, R., Yang, X., 2020. Estimating River Sediment Discharge in the Upper Mississippi River Using Landsat Imagery. Remote Sens. 12, 2370. https://doi.org/10.3390/rs12152370.

Food and Agriculture Organization – FAO, 2009. Grassland Index - A Searchable Catalogue of Grass and Forage Legumes. Food and Agriculture Organization of the United Nations, Rome. https://web.archive.org/web/20081024221053/http://www.fao.org/ag/AGP/AGPC/doc/Gbase/data/pf000187.htm (acesso em 15 de outubro de 2020).

Food and Agriculture Organization – FAO, 2016. NASA SERVIR team learn about FAO monitoring software. http://www.fao.org/forestry/news/91977/en/. (acesso em 08 de agosto de 2020)

Gitelson, A.A., 2004. Wide Dynamic Range Vegetation Index for Remote Quantification of Biophysical Characteristics of Vegetation. J. Plant Physiol. 161, 165–173. https://doi.org/10.1078/0176-1617-01176.

Google Earth Engine – GEE, 2020. Case Studies. https://earthengine.google.com/case_studies/. (acesso em 15 de outubro de 2020).

Gorelick, N., Hancher, M., Dixon, M., Ilyushchenko, S., Thau, D., Moore, R., 2017. Google Earth Engine: Planetary-scale geospatial analysis for everyone. Remote Sens. Environ. 202, 18–27. https://doi.org/10.1016/j.rse.2017.06.031.

Hansen, M.C., Potapov, P. V., Moore, R., Hancher, M., Turubanova, S.A., Tyukavina, A.,. Thau, D., Stehman, S. V., Goetz, S.J., Loveland, T.R., Kommareddy, A., Egorov, A., Chini, L., Justice, C.O., Townshend, J.R.G., 2013. High-Resolution Global Maps of 21st-Century Forest Cover Change. Science (80-. ). 342, 850–853. https://doi.org/10.1126/science.1244693.

Henebry, G., Viña, A., Gitelson, A., 2004. The wide dynamic range vegetation index and its potential utility for gap analysis. Pap. Nat. Resour. 50–56.

Imukova, K., Ingwersen, J., Streck, T., 2015. Determining the spatial and temporal dynamics of the green vegetation fraction of croplands using high-resolution RapidEye satellite images. Agric. For. Meteorol. 206, 113–123. https://doi.org/10.1016/j.agrformet.2015.03.003.

Instituto Brasileiro de Geografia e Estatística – IBGE, 2020. https://censo2010.ibge.gov.br/sinopse/index.php?uf=31&dados=8. (acesso em 15 de outubro de 2020).

Jacquemoud, S., & Ustin, S. L., 2008. Modeling leaf optical properties. Photobiological Sciences Online. Environmental Photobiology. http://photobiology.info/#Environ. (acesso em 20 de outubro de 2020.

Jain, N., Ray, S.S., Singh, J.P., Panigrahy, S., 2007. Use of hyperspectral data to assess the effects of different nitrogen applications on a potato crop. Precis. Agric. 8, 225–239. https://doi.org/10.1007/s11119-007-9042-0.

Jang, G., Kim, J., Yu, J.-K., Kim, H.-J., Kim, Y., Kim, D.-W., Kim, K.-H., Lee, C.W., Chung, Y.S., 2020. Review: Cost-Effective Unmanned Aerial Vehicle (UAV) Platform for Field Plant Breeding Application. Remote Sens. 12, 998. https://doi.org/10.3390/rs12060998.

Jiang, H., Xu, X., Guan, M., Wang, L., Huang, Y., Jiang, Y., 2019. Determining the contributions of climate change and human activities to vegetation dynamics in agro-pastural transitional zone of northern China from 2000 to 2015. Sci. Total Environ. 718, 134871. https://doi.org/10.1016/j.scitotenv.2019.134871.

Junges, A.H., Bremm, C., Fontana, D.C., Oliveira, C.A.O. de, Schaparini, L.P., Carvalho, P.C. de F., 2016. Temporal profiles of vegetation indices for characterizing grazing intensity on natural grasslands in Pampa biome. Sci. Agric. 73, 332–337. https://doi.org/10.1590/0103-9016-2015-0213.

Karnieli, A., Bayarjargal, Y., Bayasgalan, M., Mandakh, B., Dugarjav, C., Burgheimer, J., Khudulmur, S., Bazha, S.N., Gunin, P.D., 2013. Do vegetation indices provide a reliable indication of vegetation degradation? A case study in the Mongolian pastures. Int. J. Remote Sens. 34, 6243–6262. https://doi.org/10.1080/01431161.2013.793865.

Katsoulas, N., Elvanidi, A., Ferentinos, K.P., Kacira, M., Bartzanas, T., Kittas, C., 2016. Crop reflectance monitoring as a tool for water stress detection in greenhouses: A review. Biosyst. Eng. 151, 374–398. https://doi.org/10.1016/j.biosystemseng.2016.10.003.

Kim, S.L., Chung, Y.S., Ji, H., Lee, H., Choi, I., Kim, N., Lee, E., Oh, J., Kang, D.-Y., BAEK, J., Lee, G.-S., Kwon, T.-R., Kim, K.-H., 2019. New Parameters for Seedling Vigor Developed via Phenomics. Appl. Sci. 9, 1752. https://doi.org/10.3390/app9091752.

Lei Estadual de Minas Gerais nº 13.183/1999, 1999. https://documentacao.socioambiental.org/ato_normativo/UC/4482_20200510_223340.pdf. (acesso em 15 de outubro de 2020).

Li, S., Verburg, P.H., Lv, S., Wu, J., Li, X., 2012. Spatial analysis of the driving factors of grassland degradation under conditions of climate change and intensive use in Inner Mongolia, China. Reg. Environ. Chang. 12, 461–474. https://doi.org/10.1007/s10113-011-0264-3.

Li, S., Yuan, F., Ata-UI-Karim, S.T., Zheng, H., Cheng, T., Liu, X., Tian, Y., Zhu, Y., Cao, W., Cao, Q., 2019. Combining color indices and textures of UAV-based digital imagery for rice LAI estimation. Remote Sens. 11. https://doi.org/10.3390/rs11151763.

Li, X., Gao, Z., Bai, L., Huang, Y., 2012. Potential of High Resolution Rapideye Data for Sparse Vegetation. Geosci. Remote Sens. Symp. (IGARSS), 2012 IEEE Int. 420–423. https://doi.org/10.1109/IGARSS.2012.6351548.

Liu, J., Pattey, E., 2010. Retrieval of leaf area index from top-of-canopy digital photography over agricultural crops. Agric. For. Meteorol. 150, 1485–1490. https://doi.org/10.1016/j.agrformet.2010.08.002.

Louhaichi, M., Borman, M.M., Johnson, D.E., 2001. Spatially Located Platform and Aerial Photography for Documentation of Grazing Impacts on Wheat. Geocarto Int. 16, 65–70. https://doi.org/10.1080/10106040108542184.

Lu, D., Weng, Q., 2007. A survey of image classification methods and techniques for improving classification performance. Int. J. Remote Sens. 28, 823–870. https://doi.org/10.1080/01431160600746456.

Macedo, M.C.M.., Zimmer, A.H.., Kichel, A.N.., Almeida, R.G.., Araujo, A.R., 2014. Degradação de pastagens, alternativas de recuperação e renovação, e formas de mitigação. Encontro adubaçao pastagens da Scot Consult. - Tec - Fértil. 158–181.

Mapbiomas. MapBiomas General "Handbook" Algorithm Theoretical Basis Document (ATBD), 2019. https://mapbiomas-br-site.s3.amazonaws.com/ATBD_Collection_4_v2_Dez2019.pdf. (acesso em 08 de agosto de 2020).

Marcial-Pablo, M. de J., Gonzalez-Sanchez, A., Jimenez-Jimenez, S.I., Ontiveros-Capurata, R.E., Ojeda-Bustamante, W., 2019. Estimation of vegetation fraction using RGB and multispectral images from UAV. Int. J. Remote Sens. 40, 420–438. https://doi.org/10.1080/01431161.2018.1528017.

Martins, G. A., Domingues, O, 2014. Estatística Geral e Aplicada. 5ª ed. rev. e ampl. – São Paulo: Atlas.

Melo, V.F., Corrêa, G.F., Maschio, P.A., Ribeiro, A.N., Lima, V.C., 2003. Importância das espécies minerais no potássio total da fração argila de solos do Triângulo Mineiro. Rev. Bras. Ciência do Solo 27, 09–10. https://doi.org/10.1590/S0100-06832003000500005.

Meneses, P.R., Almeida, T. De, Macedo, G.B.D.M., 2019. REFLECTÂNCIA DOS MATERIAIS TERRESTRES: ANÁLISE E INTERPRETAÇÃO. Oficina de Textos, São Paulo - SP.

Merzlyak, M.N., Gitelson, A.A., Chivkunova, O.B., Solovchenko, A.E., Pogosyan, S.I., 2003. Application of Reflectance Spectroscopy for Analysis of Higher Plant Pigments. Russ. J. Plant Physiol. 50, 704–710. https://doi.org/10.1023/A:1025608728405.

Meyer, G.E., Neto, J.C., 2008. Verification of color vegetation indices for automated crop imaging applications. Comput. Electron. Agric. 63, 282–293. https://doi.org/10.1016/j.compag.2008.03.009.

Monteiro, E. de C., Burak, D.L., Cunha, A. de M., Passos, R.R., Mendonça, E. de S., 2018. Visual assessment of pasture degradation: validation by ground cover and seasonal variation. Rev. CIÊNCIA AGRONÔMICA 49, 174–182. https://doi.org/10.5935/1806-6690.20180020.

Müller, H., Rufin, P., Griffiths, P., Barros Siqueira, A.J., Hostert, P., 2015. Mining dense Landsat time series for separating cropland and pasture in a heterogeneous Brazilian savanna landscape. Remote Sens. Environ. 156, 490–499. https://doi.org/10.1016/j.rse.2014.10.014.

Nakashima, M.R., Alves, G.B., Barreiros, A.M., Queiroz Neto, J.P., 2017. DOS SOLOS À PAISAGEM: UMA DISCUSSÃO TEÓRICO-METODOLÓGICA. Rev. da Anpege 13, 30–52. https://doi.org/10.5418/RA2017.1320.0003.

Netto, J. da S.M., Baptista, G.M. de M., 2000. Reflectância espectral de solos. Doc. - Embrapa Cerrados, Planaltina - DF.

Neves, A.K., 2017. Mineração de dados de sensoriamento remoto para detecção e classificação de áreas de pastagem na amazônia legal. Diss. (Mestrado em Sensoriamento Remoto) – Inst. Nac. Pesqui. Espac. São José dos Campos, 2017. Orientadores Drs. Thales Sehn Körting, e Leila Maria Garcia Fonseca.

Nishiyama, L., 1998. Procedimentos de mapeamento geotécnico como base para análises e avaliações ambientais do meio físico, em escala 1:100.000: aplicação no município de Uberlândia - MG. São Carlos: UFSCar, 1998.

Novo, E.M.L. de M., Ponzoni, F.J., 2001. Introdução ao sensoriamento remoto. São José dos Campos.

Peñuelas, J., Filella, I., 1998. Visible and near-infrared reflectance techniques for diagnosing plant physiological status. Trends Plant Sci. 3, 151–156. https://doi.org/10.1016/S1360-1385(98)01213-8.

PMU, P.D.U., CODAU, C.O. de D. e S. de U., 2006. PROJETO ÁGUA VIVA - Relatório ambiental. Uberaba - MG. http://uberaba.mg.gov.br/portal/acervo/agua_viva/arquivos/avaliacao_ambiental/Relatorio%20Ambiental%201.pdf. (acesso em 19 de agosto de 2020).

Postel, S.L., 1998. Water for Food Production: Will There Be Enough in 2025? Bioscience 48, 629–637. https://doi.org/10.2307/1313422.

Qiu, Z., Xiang, H., Ma, F., Du, C., 2020. Qualifications of rice growth indicators optimized at different growth stages using unmanned aerial vehicle digital imagery. Remote Sens. 12, 1–18. https://doi.org/10.3390/rs12193228.

Quinino, R.C., Reis, E.A., Bessegato, L.F., 1991. O Coeficiente de Determinação $R^2$ como Instrumento Didático para Avaliar a Utilidade de um Modelo de Regressão Linear Múltipla.

Ren, Y., Zhang, W., Huang, Y., Zhang, Y., Wang, J., Yang, M., 2020. Transcriptome analysis reveals that Populus tomentosa hybrid poplar 741 responds to blue light treatment by regulating growth-related genes and their metabolic pathways. Ind. Crops Prod. 152, 112512. https://doi.org/10.1016/j.indcrop.2020.112512.

Rocha Junior, P.R. da, Andrade, F.V., Mendonça, E. de S., Donagemma, G.K., Fernandes, R.B.A., Bhattharai, R., Kalita, P.K., 2016. Soil, water, and nutrient losses from management alternatives for degraded pasture in Brazilian Atlantic Rainforest biome. Sci. Total Environ. 583, 53–63. https://doi.org/10.1016/j.scitotenv.2016.12.187.

Rubira, F.G., Barreiros, A.M., Villela, F.N.J., Perez Filho, A., 2019. Pedogeomorphological systems in the interpretation of the evolution of quaternary landscapes in humid tropical climates. Mercator 18, 1–16. https://doi.org/10.4215/rm2019.e18020.

Sanchez, G., 2013. PLS Path Modeling with R. Trowchez Ed. 235.

Santos, H.G. dos, Jacomine, P.K.T., Anjos, L.H.C. dos, Oliveira, V.Á. de, Lumbreras, J.F., Coelho, M.R., Almeida, J.A. de, Filho, J.C. de A., Oliveira, J.B. de, Cunha, T.J.F., 2018. Sistema brasileiro de classificação de solos, Embrapa Solos.
São Paulo.

Schlemmer, M.R., Francis, D.D., Shanahan, J.F., Schepers, J.S., 2005. Remotely Measuring Chlorophyll Content in Corn Leaves with Differing Nitrogen Levels and Relative Water Content. Agron. J. 97, 106–112. https://doi.org/10.2134/agronj2005.0106.

Silva, G.C. da, 2017. Detecção e contagem de plantas utilizando técnicas de inteligência artificial e machine learning. Trab. Conclusão Curso submetido ao Departamento Eng. Elétrica e Eletrônica da Univ. Fed. St. Catarina para a obtenção do título Bacharel em Eng. Eletrônica.

Silva, L.S., Marques Júnior, J., Barrón, V., Gomes, R.P., Teixeira, D.D.B., Siqueira, D.S., Vasconcelos, V., 2020. Spatial variability of iron oxides in soils from Brazilian sandstone and basalt. CATENA 185, 104258. https://doi.org/10.1016/j.catena.2019.104258.

Sipos, L., Boros, I.F., Csambalik, L., Székely, G., Jung, A., Balázs, L., 2020. Horticultural lighting system optimalization: A review. Sci. Hortic. (Amsterdam). 273, 109631. https://doi.org/10.1016/j.scienta.2020.109631.

Siqueira, H.E., Pissarra, T.C.T., do Valle Junior, R.F., Fernandes, L.F.S., Pacheco, F.A.L., 2017. A multi criteria analog model for assessing the vulnerability of rural catchments to road spills of hazardous substances. Environ. Impact Assess. Rev. 64, 26–36. https://doi.org/10.1016/j.eiar.2017.02.002.

Souza, C.H.W. DE, 2013. Estimativa de área de soja e milho cultivado no estado do paraná utilizando-se do perfil espectro-temporal de índices de vegetação. Diss. apresentada ao Programa Pós-Graduação em Eng. Agrícola para obtenção do título Mestre em Eng. Agrícola, área Conc. Sist. Biológicos e Agroindustriais, com a temática Geoprocessamento, Estatística Espac. e Agric 95.

Sun, B., Li, Z., Gao, W., Zhang, Y., Gao, Z., Song, Z., Qin, P., Tian, X., 2019. Identification and assessment of the factors driving vegetation degradation/regeneration in drylands using synthetic high spatiotemporal remote sensing Data—A case study in Zhenglanqi, Inner Mongolia, China. Ecol. Indic. 107, 105614. https://doi.org/10.1016/j.ecolind.2019.105614.

Taiz, L., Zeiger, E., 2017. Fisiologia e desenvolvimento vegetal, 6ª Edição, Porto Alegre: Artmed.

Torres, F.N. de, Richter, R., Vohland, M., 2019. A multisensoral approach for high-resolution land cover and pasture degradation mapping in the humid tropics: A case study of the fragmented landscape of Rio de Janeiro. Int. J. Appl. Earth Obs. Geoinf. 78, 189–201. https://doi.org/10.1016/j.jag.2019.01.011.

Townsend, C.R., Costa, N.L., Pereira, R.G.A., 2012. Recuperação e práticas sustentáveis de manejo de pastagens na Amazônia, Documentos. Porto Velho - RO.

Universidade Federal de Viçosa – UFV, 2010. Mapa de solos do Estado de Minas Gerais. Belo Horizonte, Fundação Estadual do Meio Ambiente. 49p. http://www.dps.ufv.br/?page_id=742. (acesso em 15 de outubro de 2020).

Valera, C.A., Pissarra, T.C.T., Martins Filho, M.V., Valle Junior, R.F., Sanches Fernandes, L.F., Pacheco, F.A.L., 2017. A legal framework with scientific basis for applying the 'polluter pays principle' to soil conservation in rural watersheds in Brazil. Land use policy 66, 61–71. https://doi.org/10.1016/j.landusepol.2017.04.036.

Valle Júnior, R.F. do, Siqueira, H.E., Valera, C.A., Oliveira, C.F., Sanches Fernandes, L.F., Moura, J.P., Pacheco, F.A.L., 2019. Diagnosis of degraded pastures using an improved NDVI-based remote sensing approach: An application to the Environmental

Protection Area of Uberaba River Basin (Minas Gerais, Brazil). Remote Sens. Appl. Soc. Environ. 14, 20–33. https://doi.org/10.1016/j.rsase.2019.02.001.

Vigneau, N., Ecarnot, M., Rabatel, G., Roumet, P., 2011. Potential of field hyperspectral imaging as a non destructive method to assess leaf nitrogen content in Wheat. F. Crop. Res. 122, 25–31. https://doi.org/10.1016/j.fcr.2011.02.003.

Wang, J., Xiao, X., Bajgain, R., Starks, P., Steiner, J., Doughty, R.B., Chang, Q., 2019. Estimating leaf area index and aboveground biomass of grazing pastures using Sentinel-1, Sentinel-2 and Landsat images. ISPRS J. Photogramm. Remote Sens. 154, 189–201. https://doi.org/10.1016/j.isprsjprs.2019.06.007.

Wiesmair, M., Feilhauer, H., Magiera, A., Otte, A., Waldhardt, R., 2016. Estimating Vegetation Cover from High-Resolution Satellite Data to Assess Grassland Degradation in the Georgian Caucasus. Mt. Res. Dev. 36, 56–65. https://doi.org/10.1659/MRD-JOURNAL-D-15-00064.1.

Woebbecke, D.M., Meyer, G.E., Von Bargen, K., Mortensen, D.A., 1995. Color indices for weed identification under various soil, residue, and lighting conditions. Trans. Am. Soc. Agric. Eng. 38, 259–269. https://doi.org/10.13031/2013.27838.

Zhumanova, M., Mönnig, C., Hergarten, C., Darr, D., Wrage-Mönnig, N., 2018. Assessment of vegetation degradation in mountainous pastures of the Western Tien-Shan, Kyrgyzstan, using eMODIS NDVI. Ecol. Indic. 95, 527–543. https://doi.org/10.1016/j.ecolind.2018.07.060.

Zimmer, A.H., Macedo, M.C.M., Kichel, A.N., Almeida, R.G. de, 2012. Degradação, recuperação e renovação de pastagens. Documentos 189.

## TABLE LEGENDS

Table 1 – Land use by geology and respective areas in hectares. Source: Mapbiomas (2018).

| ID | Land Use and Occupation | Geological Formation | Pasture Area (ha) | Geological Area (ha) |
|---|---|---|---|---|
| 1 | Pasture | Marília | 4838.607 | 12954.619 |
| 2 | Pasture | Uberaba | 16680.859 | 27179.882 |
| 3 | Pasture | Serra Geral | 8355.814 | 12552.133 |

Tabel 2 – Compilation of geographic data used in cross-tabulation

| Data type | Purpose of the data | Source | URL |
|---|---|---|---|
| Coverage and land use map (30x30m pixel) generated from Landsat images in GEE - MAPBIOMAS collection 5.0 | Delimit the pasture area to be analyzed | Generated by accessing the GEE platform | https://code.earthengine.google.com/be6e9e5570bee31fc5574758c627f709?accept_repo=users%2Fmapbiomas%2Fuser-toolkit |
| Geological Map of the State of Minas Gerais | Separation of geologies within the EPA | State System of Environment and Water Resources | http://idesisema.meioambiente.mg.gov.br/ |
| Sheet with Zonal Statistics of ground truth sites | Regression, correlation and sensitivity analysis | (items 2.2 and 2.4) | https://code.earthengine.google.com/85c7e8d6904f747ad848d11504bae53f |
| Maps of degraded pasture in the EPA from the year 2019 | Calculation of degraded area and Crosstab analysis | (Valle Junior et al., 2019) | https://code.earthengine.google.com/e4a6f8aafd4216631d950a538fac3020 |

Source: From the author, 2021.

Table 3 – Area of mapped degraded pasture separated by the Uberaba River EPA geological formation for each vegetation index.

| Index Vegetation | Geological formation | Geology area (ha) | Pasture area (ha) | Mapped degraded area (ha) |
|---|---|---|---|---|
| NDVI | Serra Geral | 12552.1335 | 8183.4381 | 5803.0200 |
| | Marília | 12954.6193 | 4882.5330 | 2651.6700 |
| | Uberaba | 27179.8825 | 16219.7247 | 3612.2400 |
| TBQB | Serra Geral | 12552.1335 | 8183.4381 | 6792.0300 |
| | Marília | 12954.6193 | 4882.5330 | 4195.5300 |
| | Uberaba | 27179.8825 | 16219.7247 | 14192.5500 |
| TBQG | Serra Geral | 12552.1335 | 8183.4381 | 6606.8100 |
| | Marília | 12954.6193 | 4882.5330 | 3644.1900 |
| | Uberaba | 27179.8825 | 16219.7247 | 8734.3200 |
| TBQR | Serra Geral | 12552.1335 | 8183.4381 | 6212.4300 |
| | Marília | 12954.6193 | 4882.5330 | 3273.9300 |
| | Uberaba | 27179.8825 | 16219.7247 | 7999.9200 |

## FIGURE CAPTIONS

*Figure 1* – Location map of the study area.

*Figure 2* – Location map of the study area with the geological distribution and sampling points of georeferenced characterization in the field. Source: Modified from the Geological Map of the State of Minas Gerais, 2014.

*Figure 3* - Characteristics of phytophysiognomies (1 and 3, healthy pasture) and (2 and 4, degraded pasture) in the dry and rainy periods, respectively

*Figure 4* – Flowchart of the scripts

*Figure 5a* – Time series graphs of observed NDVI values and cubic regression with confidence interval to predict NDVI of the pasture, separated by geology. (a1, b1) - Serra Geral; (a2, b2) - Marília; (a3, b3) - Uberaba, being degraded on the left and healthy on the right.

*Figure 5b* – Time series graphs of observed TBQB values and cubic regression with confidence interval to predict TBQB of the pasture, separated by geology. (c1, d1) - Serra Geral; (c2, d2) - Marília; (c3, d3) - Uberaba, being degraded on the left and healthy on the right.

*Figure 5c* – Time series graphs of observed TBQG values and cubic regression with confidence interval to predict TBQG of the pasture, separated by geology. (e1, f1) - Serra Geral; (e2, f2) - Marília; (e3, f3) - Uberaba, being degraded on the left and healthy on the right.

*Figure 5d* – Time series graphs of observed TBQR values and cubic regression with confidence interval to predict TBQR of the pasture, separated by geology. (g1, h1) - Serra Geral; (g2, h2) - Marília; (g3, h3) - Uberaba, being degraded on the left and healthy on the right.

*Figure 6a* – Map of degraded pasture map in the Serra Geral formation.

*Figure 6a1* – Map of coincidence in the Serra Geral formation.

*Figure 6b* – Map of degraded pasture map in the Marília formation.

*Figure 6b1* – Map of coincidence in the Marília formation.

*Figure 6c* – Map of degraded pasture map in the Uberaba formation.

*Figure 6c1* – Map of coincidence in the Uberaba formation.

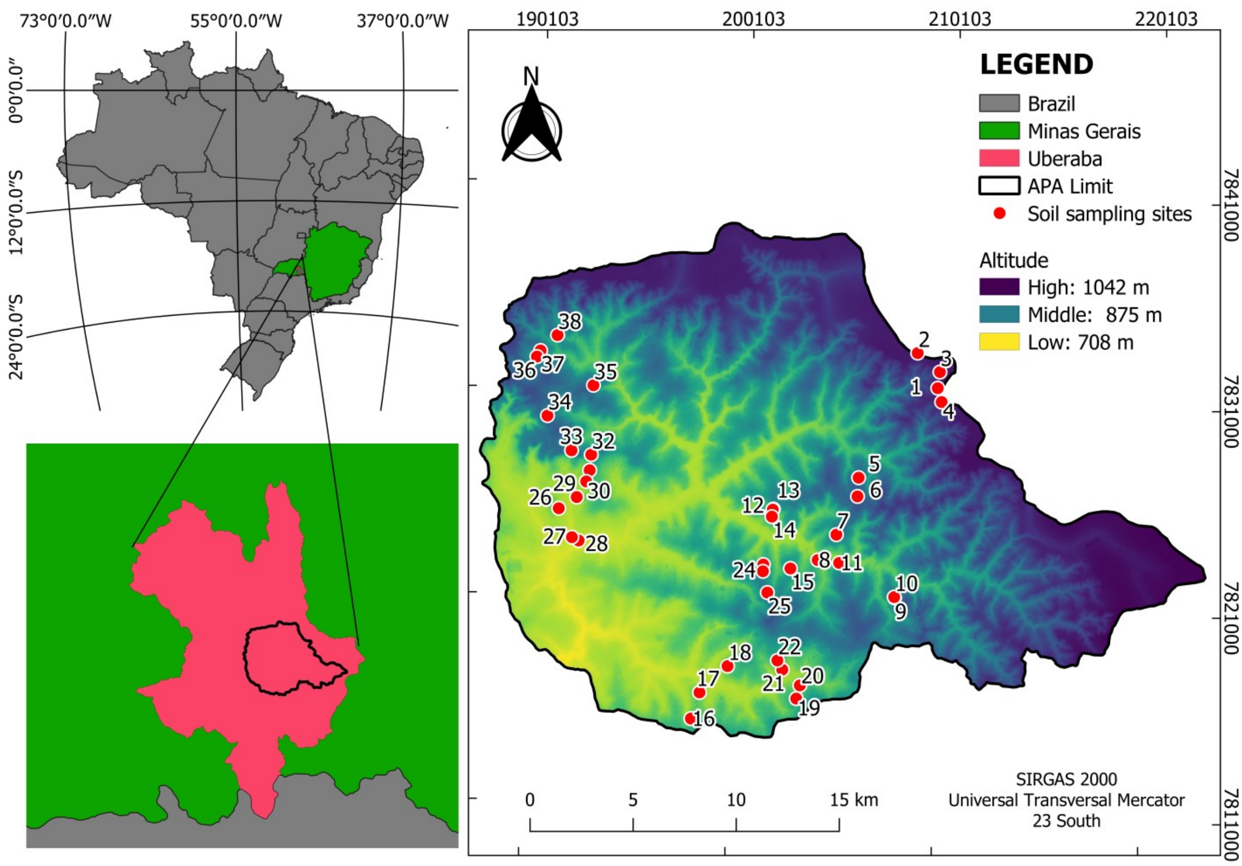


Figure 1

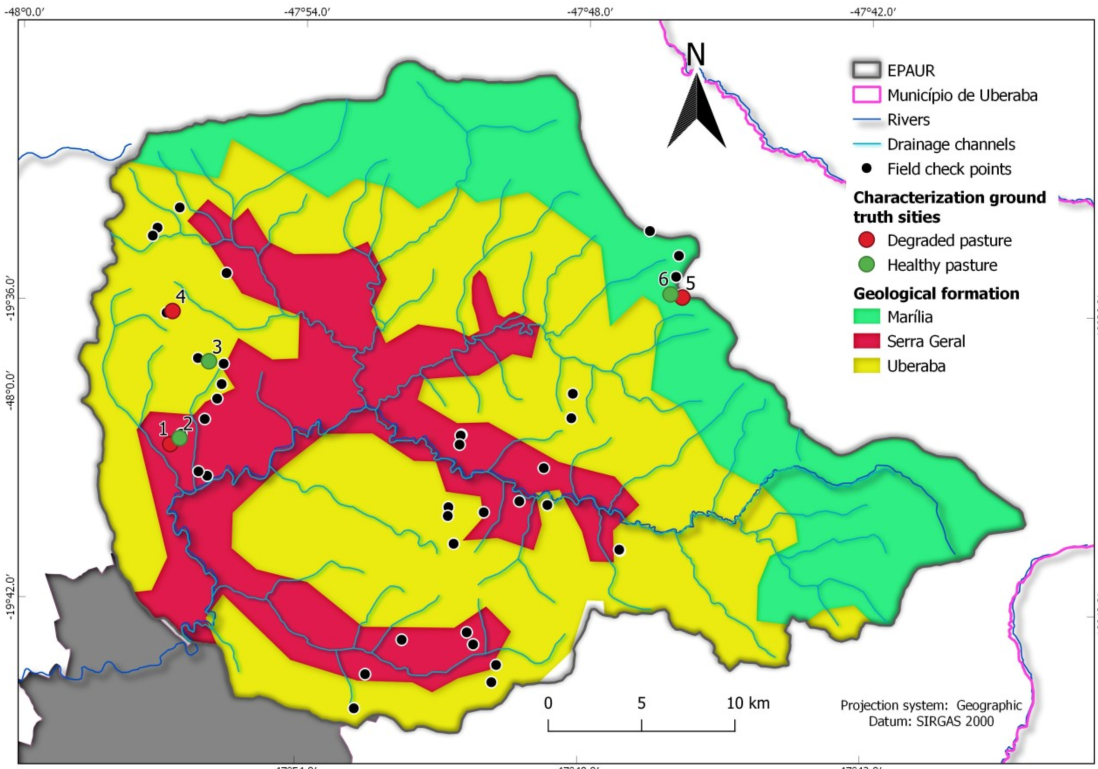


Figure 2

1 – Healthy pasture in the dry season

2 – Degraded pasture in the dry season

3 – Healthy pasture in the rainy season

4 – Degraded pasture in the rainy season

Figure 3

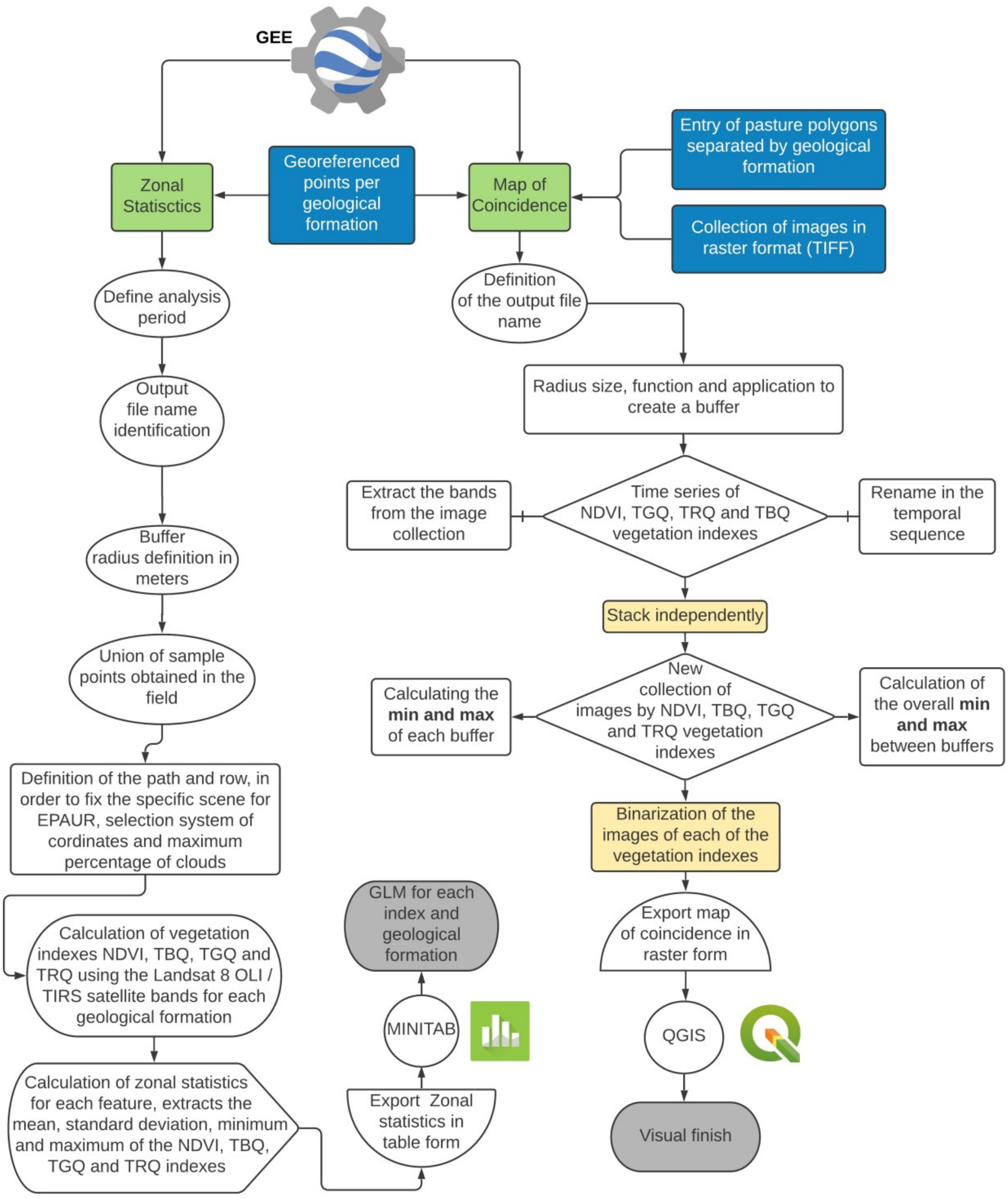
GEE
Zonal Statisctics
Georeferenced points per geological formation
Map of Coincidence
Entry of pasture polygons separated by geological formation
Collection of images in raster format (TIFF)
Define analysis period
Definition of the output file name
Output file name identification
Radius size, function and application to create a buffer
Extract the bands from the image collection
Time series of NDVI, TGQ, TRQ and TBQ vegetation indexes
Rename in the temporal sequence
Buffer radius definition in meters
Stack independently
Union of sample points obtained in the field
Calculating the min and max of each buffer
New collection of images by NDVI, TBQ, TGQ and TRQ vegetation indexes
Calculation of the overall min and max between buffers
Definition of the path and row, in order to fix the specific scene for EPAUR, selection system of cordinates and maximum percentage of clouds
Binarization of the images of each of the vegetation indexes
GLM for each index and geological formation
Export map of coincidence in raster form
Calculation of vegetation indexes NDVI, TBQ, TGQ and TRQ using the Landsat 8 OLI / TIRS satellite bands for each geological formation
MINITAB
QGIS
Calculation of zonal statistics for each feature, extracts the mean, standard deviation, minimum and maximum of the NDVI, TBQ, TGQ and TRQ indexes
Export Zonal statistics in table form
Visual finish

Figure 4

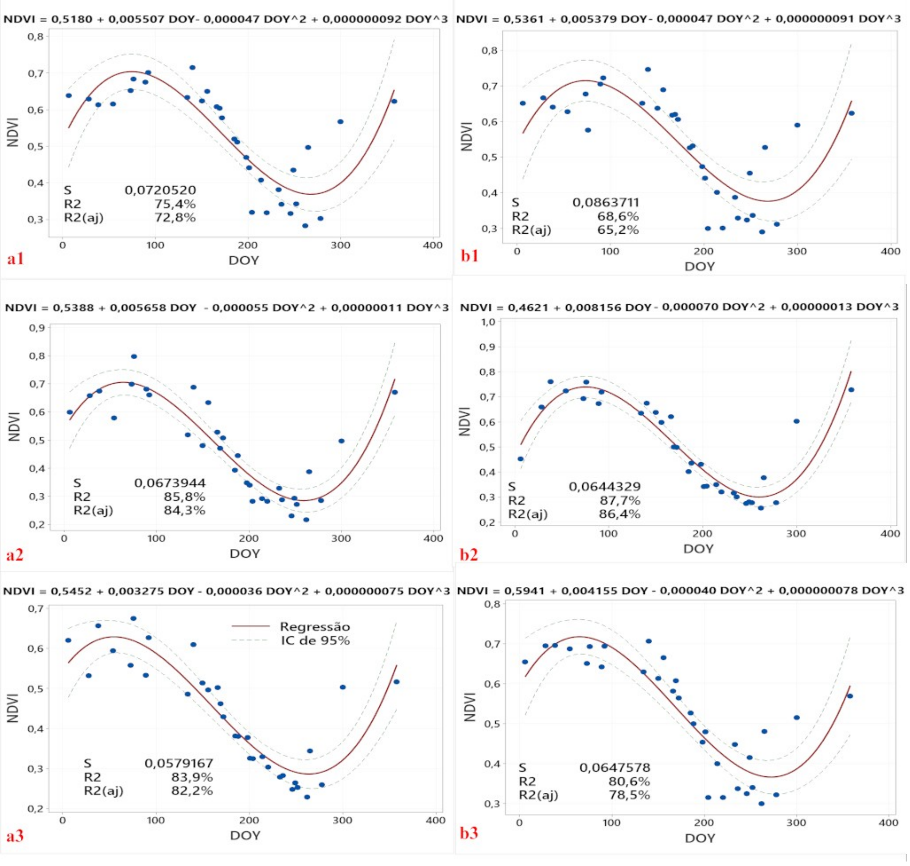


Figure 5a

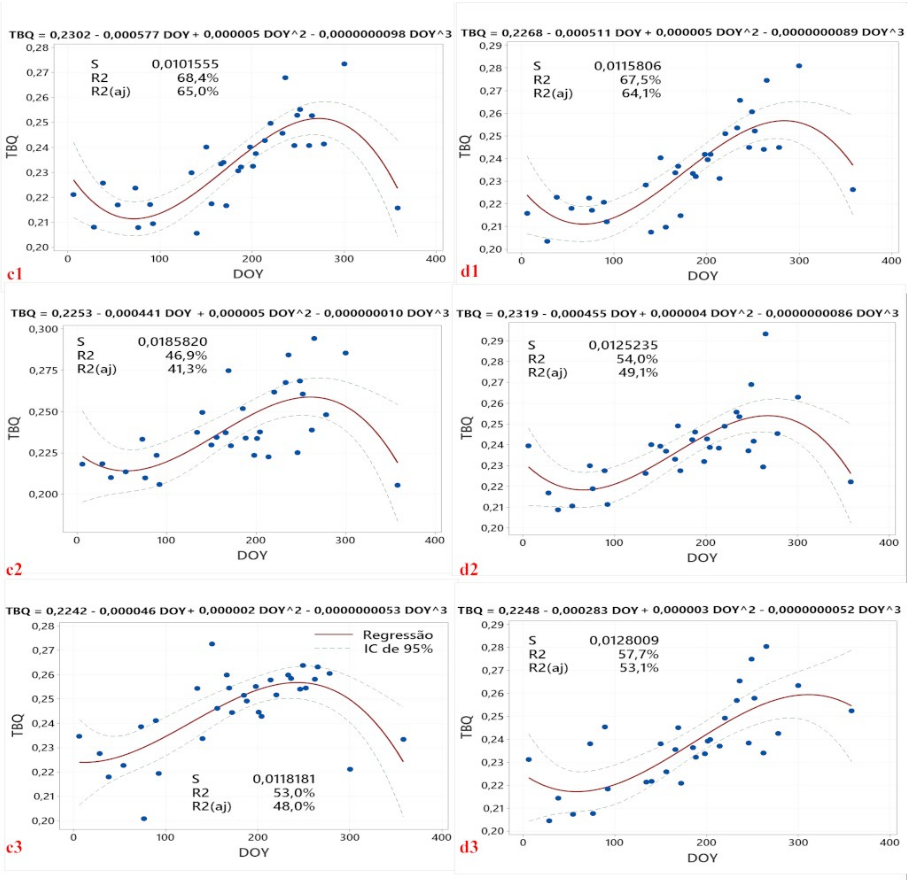


Figure 5b

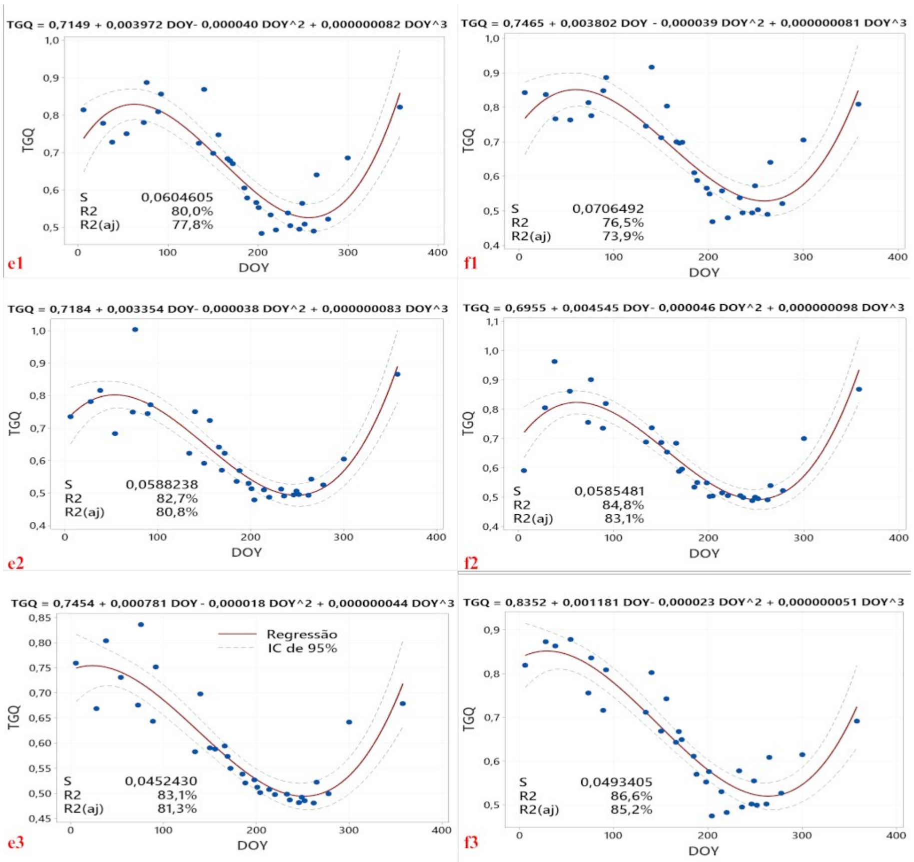
TGQ = 0,7149 + 0,003972 DOY- 0,000040 DOY^2 + 0,000000082 DOY^3
S 0,0604605
R2 80,0%
R2(aj) 77,8%
TGQ
DOY
e1
TGQ = 0,7465 + 0,003802 DOY - 0,000039 DOY^2 + 0,000000081 DOY^3
S 0,0706492
R2 76,5%
R2(aj) 73,9%
TGQ
DOY
f1
TGQ = 0,7184 + 0,003354 DOY- 0,000038 DOY^2 + 0,000000083 DOY^3
S 0,0588238
R2 82,7%
R2(aj) 80,8%
TGQ
DOY
e2
TGQ = 0,6955 + 0,004545 DOY- 0,000046 DOY^2 + 0,000000098 DOY^3
S 0,0585481
R2 84,8%
R2(aj) 83,1%
TGQ
DOY
f2
TGQ = 0,7454 + 0,000781 DOY - 0,000018 DOY^2 + 0,000000044 DOY^3
Regressão
IC de 95%
S 0,0452430
R2 83,1%
R2(aj) 81,3%
TGQ
DOY
e3
TGQ = 0,8352 + 0,001181 DOY- 0,000023 DOY^2 + 0,000000051 DOY^3
S 0,0493405
R2 86,6%
R2(aj) 85,2%
TGQ
DOY
f3

Figure 5c

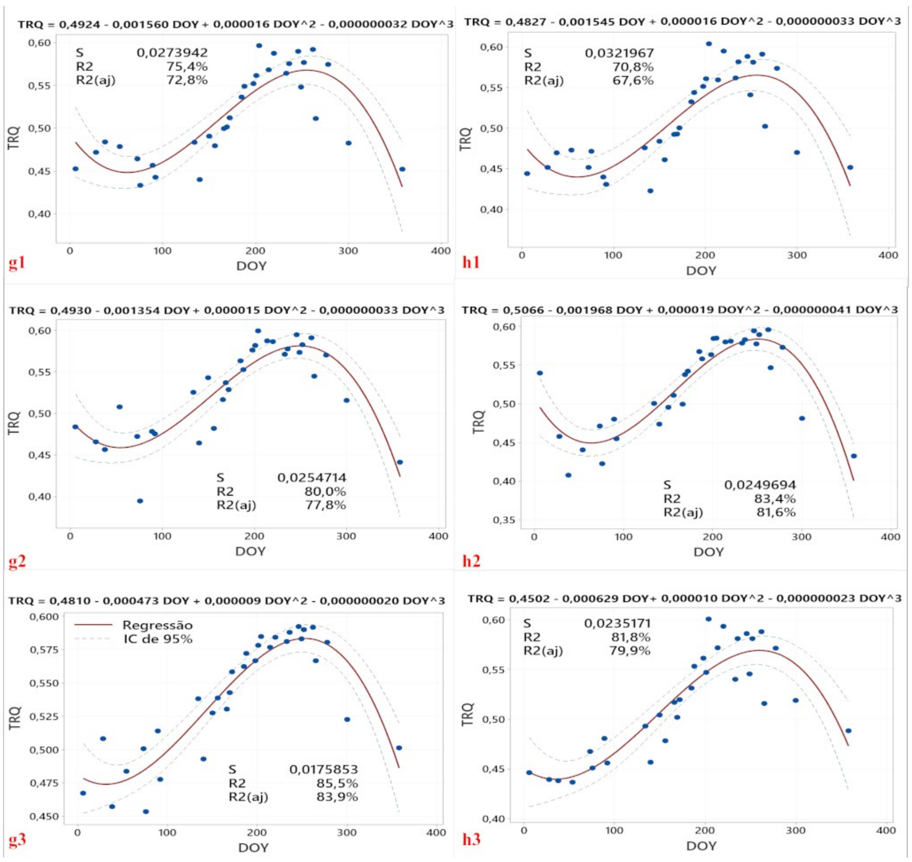
TRQ = 0,4924 - 0,001560 DOY + 0,000016 DOY^2 - 0,000000032 DOY^3
S 0,0273942
R2 75,4%
R2(aj) 72,8%
TRQ
DOY
g1
TRQ = 0,4827 - 0,001545 DOY + 0,000016 DOY^2 - 0,000000033 DOY^3
S 0,0321967
R2 70,8%
R2(aj) 67,6%
TRQ
DOY
h1
TRQ = 0,4930 - 0,001354 DOY + 0,000015 DOY^2 - 0,000000033 DOY^3
S 0,0254714
R2 80,0%
R2(aj) 77,8%
TRQ
DOY
g2
TRQ = 0,5066 - 0,001968 DOY + 0,000019 DOY^2 - 0,000000041 DOY^3
S 0,0249694
R2 83,4%
R2(aj) 81,6%
TRQ
DOY
h2
TRQ = 0,4810 - 0,000473 DOY + 0,000009 DOY^2 - 0,000000020 DOY^3
Regressão
IC de 95%
S 0,0175853
R2 85,5%
R2(aj) 83,9%
TRQ
DOY
g3
TRQ = 0,4502 - 0,000629 DOY+ 0,000010 DOY^2 - 0,000000023 DOY^3
S 0,0235171
R2 81,8%
R2(aj) 79,9%
TRQ
DOY
h3

Figure 5d

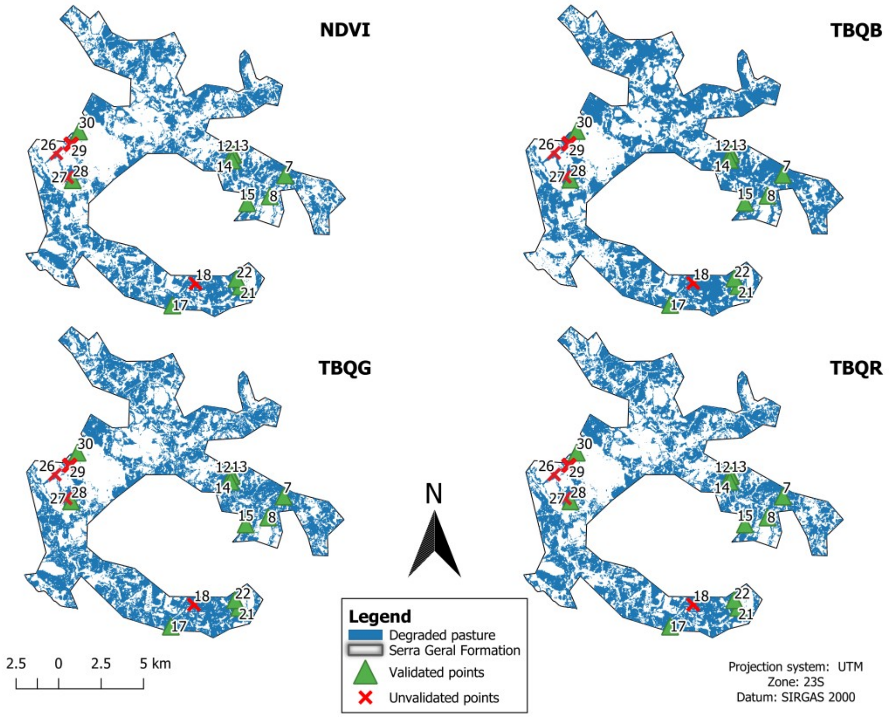


Figure 6a

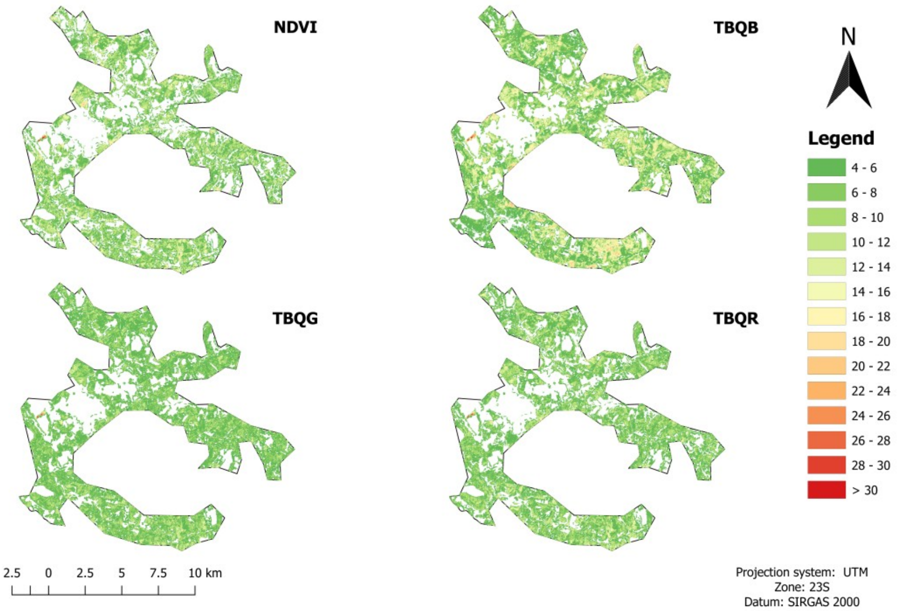


Figure 6a1

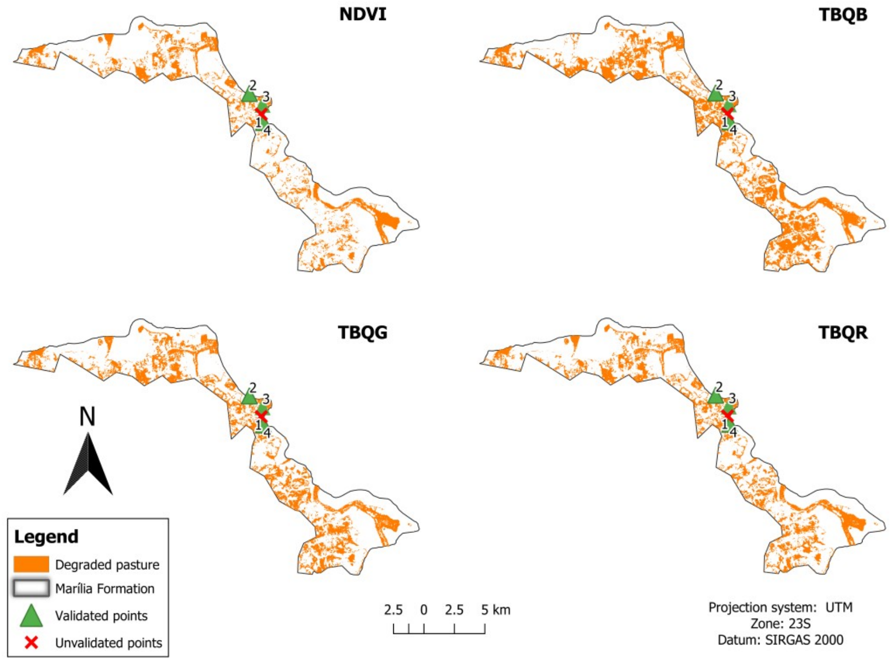


Figure 6b

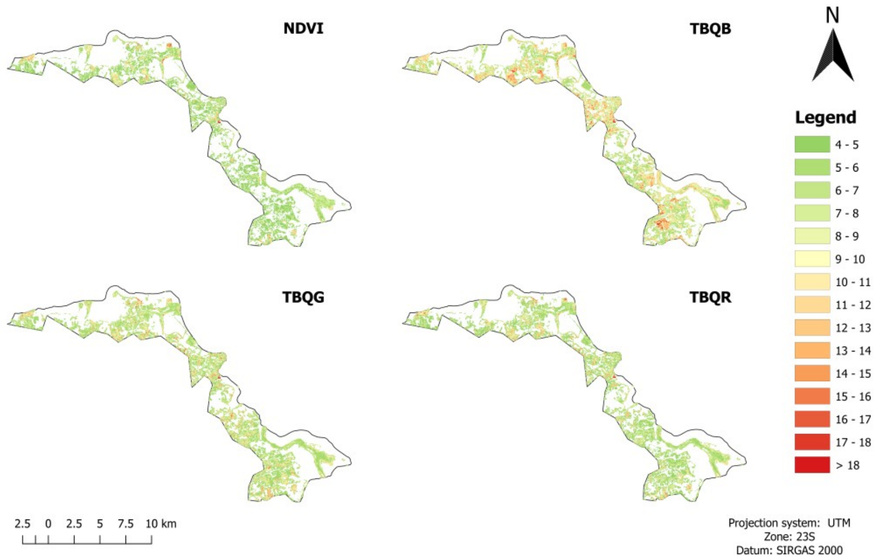


Figure 6b1

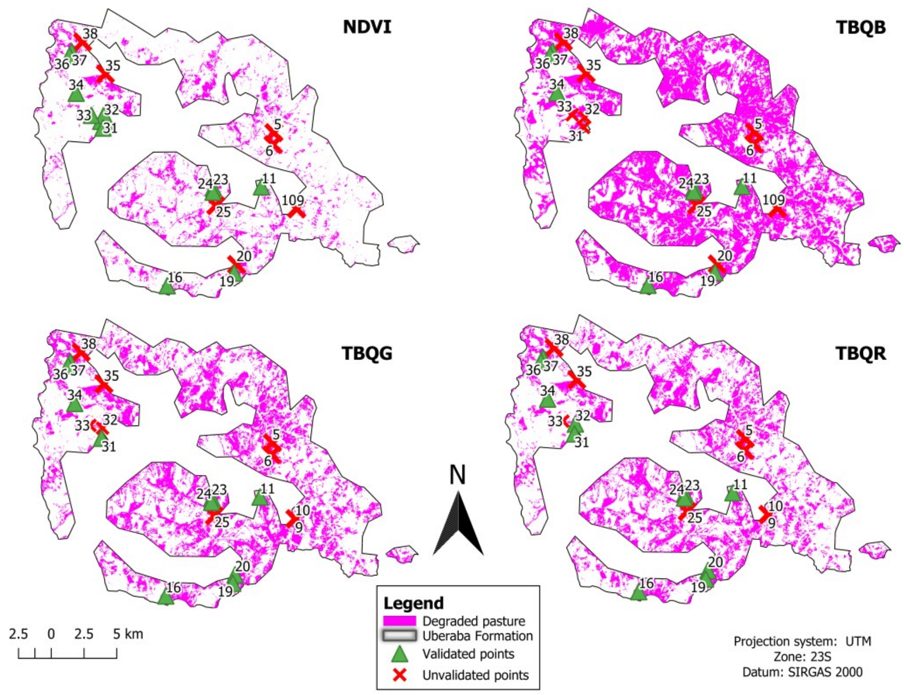


Figure 6c

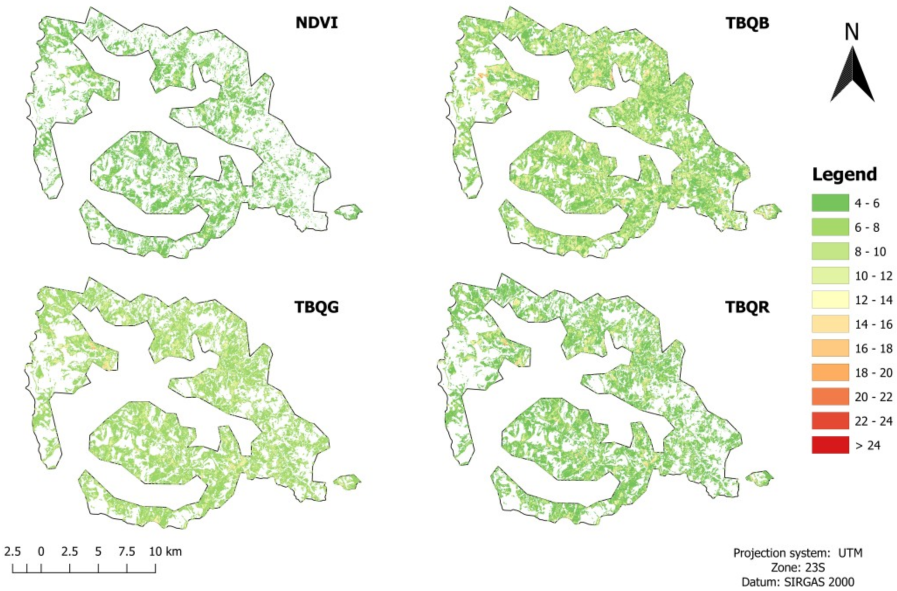


Figure 6c1